Frontiers of Information Technology & Electronic Engineering
www.jzus.zju.edu.cn; engineering.cae.cn; www.springerlink.com
ISSN 2095-9184 (print); ISSN 2095-9230 (online)
E-mail: jzus@zju.edu.cn

Design of a PCB stator coreless axial flux permanent magnet synchronous motor based on a novel topology Halbach array*

Xiao-yuan WANG, Xiang LI†‡, Chun-peng LI, Si-jia XU, Le-tao LING

College of Electrical Engineering and Automation, Tianjin University, Tianjin 300072, China

†E-mail: johnlix@163.com

Received June 2, 2017; Revision accepted Sept. 13, 2017; Crosschecked Mar. 14, 2019

Abstract: A novel topology Halbach permanent magnet array is proposed and applied to the design of a printed circuit board (PCB) axial flux permanent magnet (AFPM) motor. Compared with the traditional coreless AFPM motor, this novel topology for a Halbach permanent magnet array PCB stator AFPM motor has larger air-gap magnetic flux density and air-gap flux per pole. The magnetic flux leakage is effectively reduced, and the air-gap magnetic density is close to the sine wave. Results of the finite element analysis and prototype experiments verify the feasibility and effectiveness of the novel Halbach permanent magnet array PCB stator motor. A reference basis and practical value for the design of the PCB AFPM motor are provided.

Key words: Axial flux permanent magnet synchronous motor; Printed circuit board; Halbach permanent magnet array; Finite element method

https://doi.org/10.1631/FITEE.1700345 **CLC number:** TM351

1 Introduction

An axial flux permanent magnet (AFPM) motor is different from a radial flux permanent magnet motor because the air-gap flux is along the axial direction and the air gap is in-plane (Tang, 1997). Because its axial dimension and the armature winding inductance are small (Dutta and Rahman, 2008), AFPM has received increased attention (Wang et al., 2007). AFPM motor performs well as a servo motor and is widely used in electric vehicles (Kumar et al., 2014), wind power (Neethu et al., 2010), aerospace, and other fields (Fan and Wu, 2010). A printed circuit board (PCB) stator coreless AFPM motor can greatly reduce the weight of the motor with no cogging torque (Kumar et al., 2015) or stator iron loss, and can achieve an accurate position of the coil (Yu et al., 2011); thus, the motor servo is good and conducive for batch production (Wu, 2012). However, flux in the stator coils will be reduced because of the coreless stator structure (Zhu et al., 2013); thus, there are many design requirements for the air-gap magnetic flux density, and the air-gap magnetic density is close to the sine wave. In contrast to the traditional AFPM motor, stator winding of the PCB stator is directly printed on the PCB. In a certain area of PCB, the numbers of turns of stator winding, line width, and line distance are different. To give the PCB a certain flow capacity, considering heat dissipation, the PCB plate must have a certain thickness; thus, the air-gap length is not too small. Considering the weight of the motor, the cost, and axial length of the rotor stator, the PCB motor should not be too thick. Optimizing the distribution of poles on the rotor magnetic steel has become a preferred method to improve the performance of a PCB stator motor (Cao et al., 2014).

A Halbach permanent magnet array has been widely used in the design of permanent magnet motors (Galea et al., 2015), and some researchers have studied this array (Huang et al., 2017). Jiao et al.

‡ Corresponding author

* Project supported by the National Natural Science Foundation of China (No. 51577125)

ORCID: Xiang LI, http://orcid.org/0000-0002-3022-617x

(2017) studied the applicability of the Halbach array on the AFPM motor, the influence of the magnetization angle of this array on air-gap flux density, and the performance of the AFPM motor. A coreless AFPM motor was designed using a Halbach permanent magnet array (Zheng et al., 2010). Two-dimensional (2D) simulation results were compared with 3D ones. The influences of 45°, 60°, and 90° Halbach permanent magnet arrays on the air-gap magnetic flux density and torque density were analyzed (Ubani et al., 2016). However, simulation analysis instead of experimental verification was performed. The magnetic vector potential of the Halbach permanent magnet array magnetic field was analyzed and applied to the coreless permanent magnet synchronous linear motor, showing that the harmonic was significantly weakened and that the amplitude of the back electromotive force (EMF) slightly decreased (Zhang et al., 2013). The fundamental maximum/minimum amplitude hybrid with a global optimization algorithm for multiple objectives and the sine distortion rate were discussed, and the magnetic pole angle and magnetizing angle of the air-gap flux density waveform of the fundamental amplitude and harmonic distortion were studied (Fan et al., 2009). In addition, some works improved the performance of the AFPM using Halbach arrays by changing the permanent magnet materials; however, this method will lead to a cost increase of the motor (Luise et al., 2016). The effect of the motor's permanent magnet array on different lengths of the air gap and the thickness of the permanent magnet on the application of the Halbach were studied by changing only the Halbach permanent magnet array angle instead of the Halbach permanent magnet array shape (Li et al., 2015). Studies of the Halbach permanent magnet array used in the AFPM motor focus on the magnetization angle of the magnet steel, the thickness ratio of the magnetic steel, and the back iron. The influence of the shape of the array on the air-gap magnetic flux density and magnetic flux leakage, especially from the inner and outer diameters of the rotor, has received little attention.

In this study, we propose a design of a PCB stator coreless AFPM motor rotor structure. Using a novel topology for a Halbach permanent magnet array, where the pole diameter and outer diameter of the polar angle parameters are independent, the main and auxiliary poles are optimized with different central fan shapes, and the main and auxiliary pole distributions of the magnet are reasonable. Assume that the amount of permanent magnetic materials does not change. Thus, the performance of the coreless AFPM motor stator of a PCB is optimized. A model with 3D electromagnetic field was established using a finite element method (FEM) method to simulate the air-gap magnetic flux density and magnetic flux leakage of the PCB stator coreless AFPM motor. The fundamental frequency and sinusoidal distortion rate of the air-gap magnetic flux density were analyzed and compared with the counterparts of the main magnetic and auxiliary magnetic poles with different shapes. A finite analysis simulation verified the accuracy of the experimental results. Thus, our method can provide a reference basis and practical value for the design of a magnetic steel structure for PCB stator coreless AFPM motors.

2 A PCB stator coreless AFPM motor and a novel Halbach array

2.1 A PCB stator AFPM motor structure

In this study, the PCB stator coreless AFPM motor is a single-stator double-rotor structure (Fig. 1), and the PCB stator is in the middle of the bilateral magnetic steel. The structure can overcome single-side tension, reduce magnetic leakage, and effectively increase the air-gap magnetic flux density. The rotor is made of type 45H neodymium iron boron permanent magnet material. The PCB stator winding uses a three-phase winding with eight layers, and each layer contains 12 coils.

2.2 Structure of a novel Halbach permanent magnet array

The Halbach permanent magnet array can increase the air-gap flux density and ensure the sine waveform of the air-gap density. It can make up the negative influence of the coreless structure on the main magnetic circuit flux and effectively increase the torque density of the motor. A traditional disk motor rotor using a Halbach permanent magnet array is shown in Fig. 2. This design uses a novel Halbach permanent magnet array, which changes the traditional Halbach permanent magnet array optimization method by adjusting the main pole in the inner and

outer diameters and the auxiliary pole in terms of arc length, i.e., the angle from the main pole in the inner and outer diameters to the center line, for an effect on the novel Halbach array's motor performance. Compared with the traditional Halbach array, the novel Halbach array makes the distribution of the main magnetic and auxiliary magnetic poles more reasonable on the magnetic steel. The novel Halbach array is used in the design of the PCB stator coreless AFPM motor, which effectively improves the sine waveform of the air-gap flux density and the no-load back EMF of the motor.

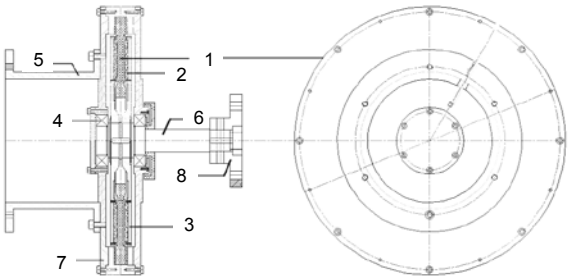

Fig. 1 Schematic of the stator slot

1: stator; 2: permanent magnet; 3: back iron; 4: bearing; 5: supporting member; 6: shaft; 7: shell; 8: prime mover

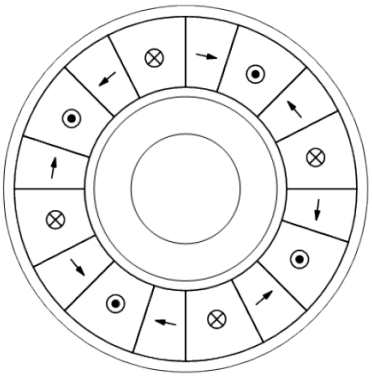

Fig. 2 Traditional 90° Halbach permanent magnet array

3 Design and analysis of the scheme

3.1 Scheme design

To analyze the air-gap flux density, the magnetic flux leakage, and no-load back EMF of the PCB stator AFPM motor, a model of the PCB stator AFPM motor is established. Parameters of the motor are shown in Table 1.

The PCB stator AFPM motor model is shown in Fig. 3. Three assumptions are made about the model:

Table 1 Basic parameters and design requirements of the motor

Parameter	Value
Rated power	200 W
Permanent magnet material model	45 H
Thickness of the permanent magnet	8 mm
Thickness of theback iron	5 mm
Rotor outer diameter	90 mm
Rotor inner diameter	52 mm
Air-gap length	5 mm
Number of turns	8
Number of slots	12
Number of pole pairs	8

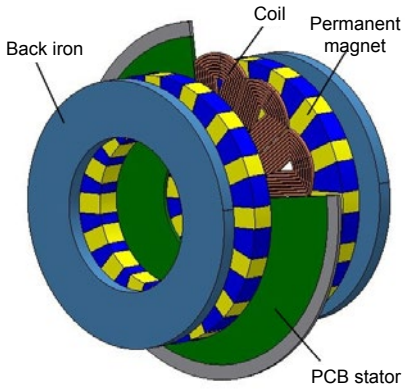

Fig. 3 PCB stator AFPM motor model

1. The permanent magnet is uniformly magnetized, the surface is smooth, and the two permanent magnets can be perfectly combined.

2. Permeabilities of the PCB stator coil and air are approximately equivalent; thus, the PCB stator coil is treated as air when the gap flux density is calculated without load.

3. The influence of the rise of temperature on the magnetism of the permanent magnet and performance of the motor is ignored.

In the design of the PCB stator AFPM motor, the correct selection of rotor size influences the size and waveform of the air-gap magnetic flux, and the cost and weight of the motor primarily depend on the size of the permanent magnet used by the rotor. Therefore, the size of the permanent magnet on the rotor disk must be optimized to achieve a sinusoidal distribution and a large amplitude air-gap flux density. This is achieved by changing the polar angle of the main magnetic and auxiliary magnetic poles from the inner

and outer diameters. To ensure that the air-gap flux density is adequate, flux leakage is reduced as much as possible; thus, the air-gap magnetic density waveform is close to a sine wave.

Compared with other AFPM motors, the PCB stator coreless AFPM motor has the following advantages because of its structure:

1. The stator disk adopting a PCB stator with the coreless structure can eliminate cogging torque and core loss, improve motor efficiency, and reduce the motor weight.

2. The magnetic steel disk using the Halbach permanent magnet array in an axial and tangential combination direction can eliminate the rotor back iron, reduce the rotor weight, and increase the air-gap flux density.

3. By arranging the permanent magnetic material's size and location in a practical manner, the sinusoidal distribution of air-gap flux density can be easily obtained, without increasing the quantity of permanent magnetic material, weakening harmonics, or reducing torque ripple.

3.2 Parameter analysis

3.2.1 Air-gap magnetic flux density analysis

The air-gap magnetic field of an axial flux motor is a 3D magnetic field, which is difficult to analyze. Here, the magnetic circuit at the average radius is analyzed.

Assuming that the magnetic material is evenly magnetized, then we have

$$\boldsymbol{B} = \mu_0(\boldsymbol{M} + \boldsymbol{H}), \tag{1}$$

where $\boldsymbol{B}$ is the magnetic flux density, $\boldsymbol{M}$ the magnetization intensity, and $\boldsymbol{H}$ the magnetic field strength.

The axial flux is equal to that of a 2D linear motor model. The x axis is along the radius, and the z axis is along the motor axis. The magnetization intensity function of the Halbach permanent magnet array can be expressed as

$$\boldsymbol{M}=\left(\frac{1}{\mu_0}B_x - H_x\right)\boldsymbol{a} + \left(\frac{1}{\mu_0}B_z - H_z\right)\boldsymbol{b}, \tag{2}$$

where $\boldsymbol{a}$ is the x-axis unit vector and $\boldsymbol{b}$ is the z-axis unit vector. The magnetic flux densities of the permanent magnet along the circumferential x axis and axial z axis of the motor are B_x and B_z, respectively, expressed as

$$B_x = \frac{4}{(2n+1)\pi}\sin\left[\frac{\pi}{2}(2n+1)\right]\sin\left[\frac{\pi}{2}(2n\alpha_\mathrm{p}+\alpha_\mathrm{p})\right], \tag{3}$$

$$B_z = \frac{4B_\mathrm{r}}{\mu_0(2n+1)\pi}\sin\left[\frac{1}{2}(2n+1)(1-\alpha_\mathrm{p})\right], \tag{4}$$

where α_p is the polar arc coefficient, and B_r is the remanence magnetic flux density of the permanent magnet.

Using Maxwell's equation, the air-gap flux density in the axial direction can be expressed as

$$B_{(x,z)}=B_\mathrm{r}\exp\left(\frac{(2n+1)\pi x}{\tau}\right)\frac{\sin\left(\frac{2\pi+1}{\tau}x\right)\cosh\left(\frac{2\pi h_\mathrm{m}}{\tau}z\right)}{\cosh\left(\frac{\pi h_\mathrm{m}}{\tau}d\right)}, \tag{5}$$

where τ is the polar distance, h_m the thickness of the permanent magnet, and d the distance between the permanent magnets on both sides.

3.2.2 Back EMF analysis of motor output

The PCB stator coil adopted in this study has a concentric spiral winding. Because the PCB stator has a coreless structure, the magnetic flux of each winding turn is different; therefore, it is necessary to separately analyze each coil.

For a single turn of the coil, the effective value of the back EMF is expressed as

$$E_\mathrm{q} = 4.44 f \Phi_\mathrm{m}, \tag{6}$$

where f is the frequency of an induced electromotive force in a conductor. Φ_m is the fundamental magnetic flux per pole of the motor, expressed as

$$\Phi_\mathrm{m} = B_\mathrm{max}\sum_{i=1}^{n} S_i, \tag{7}$$

where B_max is the fundamental amplitude of the air-gap flux density, and S_i is the effective area of the i^th turn of the coil at the pole.

The entire PCB stator can be considered as a combination of several turns of concentric coils. Therefore, the winding coefficient of each turn of the coil can be separately solved and then superimposed. The effective value of the back EMF for the entire PCB stator is

$$E=4.44fN\sum k_n\Phi_{\mathrm{m}}, \tag{8}$$

where $\sum k_n$ is the sum of the winding coefficients of all turns of the coil, and N is the number of layers of the PCB winding.

4 Analysis of finite element simulation results

4.1 Establishment of the motor solution model and evaluation function

In this study, the air-gap flux density of the novel Halbach array AFPM motor is simulated and analyzed using the FEM. Because the air-gap flux density of the disc motor continuously changes along the axial direction, the magnetic field of the motor is three-dimensional. Therefore, we use a 3D FEM to simulate and analyze the magnetic field of the motor. The PCB stator has eight plates and 12 coils. To facilitate finite element simulation, each turn conductor in the model is close to itself. The shape of the stator winding of the PCB is between a trapezoid and a circle (Fig. 4). This novel type of winding with circular winding and ladder winding is advantageous, because the electromotive forces obtained with trapezoidal windings are very small and their terminals are short. This novel type of winding can reduce the winding resistance in the load with a decrease in copper consumption, thus reducing the temperature. The winding can thus occur due to a large power density, so that the AFPM motor can improve the power density and thereby increase the torque.

Armature reaction is an important process in the motor. However, for the PCB stator AFPM motor, the effects of armature reaction are very limited, because the PCB stator winding is without core structure and limited to the PCB plate process. Therefore, the winding turns are few, and the armature reaction is difficult to influence the magnetic field formed by the rotor. Thus, the reactance produced by PCB winding is much smaller than that of PCB winding (especially at a low speed). Table 2 shows the comparison of the reactance and resistance of PCB winding at different speeds.

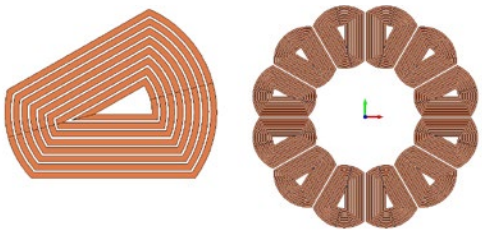

Fig. 4 PCB stator winding shape

Table 2 Winding reactance and resistance at different speeds

Speed (r/min)	X (Ω)	R (Ω)	X/R
200	0.072	1.521	0.047
300	0.107	1.521	0.070
400	0.145	1.521	0.095
500	0.174	1.521	0.114
600	0.209	1.521	0.137

The rotor model of the PCB stator motor is shown in Fig. 5. Parameters of the novel Halbach permanent magnet array magnet steel in the rotor are shown in Fig. 6. Since the motor has eight pole pairs (p=8), the motor is divided into 16 parts with 16 central lines, and the angle of each pole of the rotor, i.e., the angle between two central lines, is 2θ=360°/p. Each auxiliary magnetic pole is β_1 and β_2 in the center of the outer diameter; that is to say, $\alpha_1+\beta_1=\theta$ satisfies $\alpha_2+\beta_2=\theta$ at the same time. In case β_1 and β_2 can be changed by changing α_1 and α_2, the distribution of the main magnetic and auxiliary magnetic poles in the Halbach permanent magnet array on magnetic steel can be adjusted by changing α_1 and α_2.

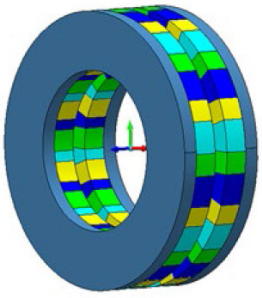

Fig. 5 Rotor model of the PCB stator motor (pole coefficient of the motor is one)

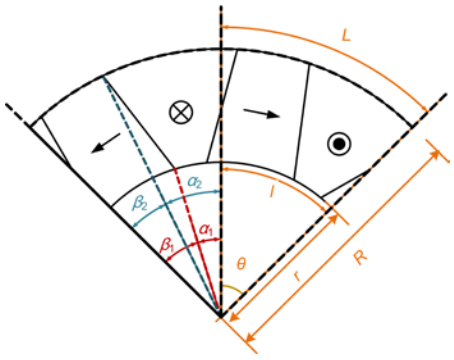

Fig. 6 Schematic of a novel Halbach permanent magnet array magnet steel

L and l are the length of the arc of the outer and inner diameters between two central lines of the magnet steel, respectively. R and r are the outer and inner diameters of the magnet steel, respectively. α_1 and α_2 are the angles between the inner magnetic pole and the outer diameter between the central line, respectively

In the design of the AFPM motor, the air-gap flux density has a direct influence on the back EMF and output torque of the motor; that is to say, the sine waveform of the air-gap flux density can reflect the flux leakage of the motor. Therefore, an evaluation function including the fundamental magnitude of the air-gap magnetic flux density and amplitude of each sub-harmonic is used as the main evaluation parameter to evaluate the feasibility of the novel Halbach permanent magnet array magnet steel, expressed as

$$F=\frac{B_{z1}}{\sqrt{B_{z3}^2+B_{z5}^2+B_{z7}^2}}, \tag{9}$$

where B_{z1} is the fundamental amplitude of the air-gap flux density along the axial direction, and B_{z3}, B_{z5}, and B_{z7} are the axial magnetic flux densities for the 3rd, 5th, and 7th harmonic amplitudes, respectively.

4.2 Influence of equal polar angles at the inner and outer diameters of the air-gap magnetic flux density

As permanent magnet price increases, to maintain the permanent magnet condition and quality, the axial and tangential magnetization of the permanent magnet can be altered by changing the angle between the main and auxiliary poles and the center line as much as possible to increase the air-gap flux density. When the polar angles of the inner and outer diameters of the permanent magnet are the same, the inside and outside contours of the permanent magnet are at the same center.

The number of pole pairs p in the motor designed in this study is eight. In the conventional axial magnetic field coreless permanent magnet motor, the permanent magnet can be magnetized along only one direction, i.e., the axial direction. The rotor of the motor in this study is a 90° Halbach array, and the center angle of each rotor is θ=360°/(2p)=22.5°. Supposing that $\alpha_1=\alpha_2=\alpha$ and $\beta_1=\beta_2=\beta$, then $\alpha+\beta$=22.5°.

A 3D electromagnetic field model is established by changing α, and the FEM is used to simulate the model. The relationship between the flux per pole and the fundamental magnitude of axial flux density is shown in Table 3.

Table 3 Relationship between the flux per pole and fundamental magnitude of axial flux density

Angle of the main magnetic pole (°)	Air-gap flux per pole ($\times10^{-4}$ Wb)	Fundamental wave amplitude of axial magnetic flux density (T)
7.25	1.34	0.868
9.25	1.38	0.920
11.25	1.45	0.945
13.25	1.41	0.931
15.25	1.39	0.884

Table 3 shows that when the air-gap flux per pole increases, the fundamental magnitude of the air-gap flux density at the mean radius of the PCB stator axial flux machine increases as well. Therefore, in the following analysis, the fundamental amplitude and the sine of the axial air-gap flux density are the main parameters to evaluate the feasibility of the magnet steel in the novel magnet array. Air-gap flux density for the pole angle changes with α at the average radius (Fig. 7). Changes in the evaluation function for different α are shown in Table 4.

Table 4 Values of evaluation functions corresponding to different α

Angle of the main magnetic pole (°)	Value of the evaluation function (F)
7.25	9.883
9.25	10.734
11.25	11.121
13.25	10.941
15.25	10.018

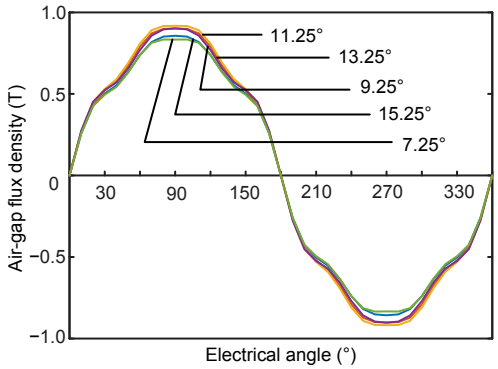

Fig. 7 Distribution of air-gap magnetic density at the mean radius of different α

Fig. 7 shows that the air-gap flux density reaches its maximum when α=11.25°, i.e., $\alpha=\beta=\theta/2$. It can also be derived from the values of evaluation function F in Table 4, and the fundamental wave has the highest energy ratio. Simulation results show the following:

1. From the synthetic waveform of the axial air-gap flux density at the mean radius, the amplitude of the air-gap flux density at α=11.25° is larger than those at α=9.25° and α=13.25°; however, the advantage of flux density at α=11.25° is not significant.

2. The evaluation function F, i.e., the fundamental wave energy ratio, is higher at α=11.25° than those at α=9.25° and α=13.25°.

We can conclude that when the main pole angle is α=11.25°, i.e., the pole angle of the axial magnetic permanent magnet is equal to that of the tangential magnetized permanent magnet, the air-gap flux density reaches its maximum and the magnetic harmonic component is the smallest.

The magnetic flux density distribution on the rotor of the motor is shown in Fig. 8. The maximum magnetic flux density of the magnet steel is 1.263 T. The analytical results of axial air-gap magnetic flux density and the simulation results are shown in Fig. 9. Fig. 9 shows that the results of the two methods are consistent with a maximum error of 0.037 T. This error is cased by the edge effect of the magnetic field. The fundamental and subharmonic components of the axial air-gap flux density are shown in Fig. 10.

In the case of the same permanent magnet, the fundamental magnitude of the magnetic flux density of the conventional axial magnetic field coreless PM motor was 0.825 T, and the 3rd and 5th harmonic components were 0.065 T and 0.061 T, respectively. Comparing the optimal conditions of the design of the Halbach permanent magnet array auxiliary PCB stator pole ratio of the coreless motor, the magnetic flux density of the fundamental amplitude increased by 14.5%, and the 3rd harmonic content was weakened.

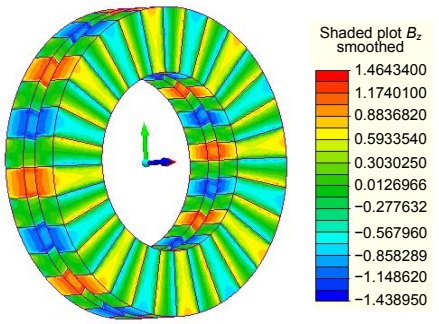

Fig. 8 Distribution of magnetic flux density of the motor rotor

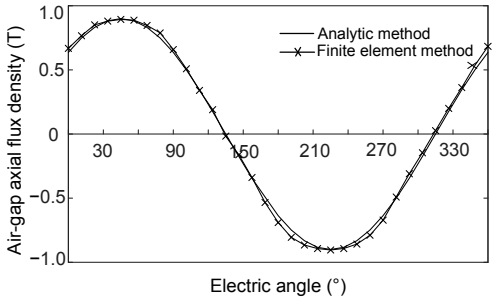

Fig. 9 Air-gap flux density waveform

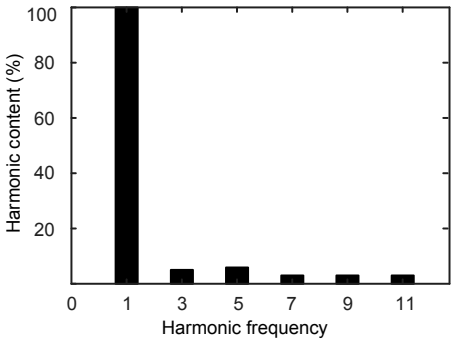

Fig. 10 Harmonic analysis of the air-gap flux density

4.3 Influence of different polar angles at the inner and outer diameters of the air-gap magnetic flux density

To increase the ratio of the permanent magnetic material, the influence of the shape and distribution of the permanent magnet on the air-gap flux density is

studied, when the inner and outer diameters of the permanent magnet, i.e., the center diameters of the permanent magnet, are different. By changing the center angle of the Halbach permanent magnet in the inner and outer diameters, α_1, α_2, β_1, and β_2 are changed, and the shape of the Halbach permanent magnet and the distribution of the magnetic steel are changed as well. Fig. 11 shows the fundamental amplitude of the axial air-gap flux density when the center of the permanent magnet is changed at the inner and outer diameters.

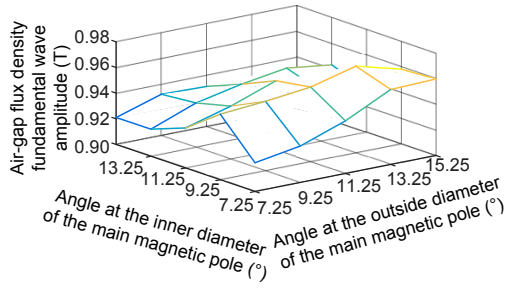

Fig. 11 Fundamental amplitude of the air-gap flux density with the center angle

Fig. 11 shows that when α_1=9.25° and α_2=13.25°, the air-gap flux density of the fundamental amplitude reaches its maximum approximately at 0.973 T. Table 5 shows the values of evaluation function F when α_1 and α_2 have different values.

Table 5 Values of the evaluation function when α_1 and α_2 have different values

α_1 (°)	α_2 (°)	Value of evaluation function (F)
7.25	13.25	11.203
7.25	15.25	11.151
9.25	13.25	11.310
9.25	15.25	11.136
13.25	9.25	10.574
15.25	9.25	10.477

Table 5 shows that when α_1=9.25° and α_2=13.25°, the value of evaluation function F reaches its maximum. When $\alpha_1<\theta/2$ and $\alpha_2>\theta/2$, the value of evaluation function F is larger than the optimization results in Section 4.2. Thus, for a PCB stator coreless AFPM motor with a Halbach permanent magnet array in the axial magnetized permanent magnet and tangential magnetized permanent magnet for equal central angle width, the axial magnetized permanent magnet can be increased in the outer diameter of the arc length, and the reduction in the inner diameter in the arc length of the gas can be accounted for. The air-gap flux density is effectively increased and the magnetic leakage is reduced. The reduction of the polar angle of the axial magnetized permanent magnet at the inner diameter and the increase in the polar angle at the outside diameter are both approximately 2°.

When α_1=9.25° and α_2=13.25°, the value of evaluation function F reaches its maximum. The flux density distribution is shown in Fig. 12 for the position of the motor magnetic air-gap at this time.

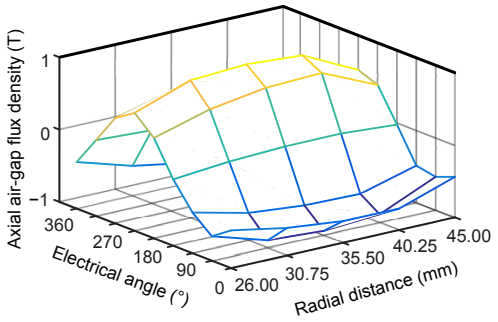

Fig. 12 Air-gap flux density at different radial positions and electrical angles

As shown in Fig. 12, the air-gap flux density increases and then decreases along the radius direction, showing a sinusoidal trend along the circumferential direction. In this case, the fundamental magnitude of the air-gap flux density and the magnitude of each subharmonic wave were compared with the optimum results in Section 4.2. The contrast diagram at α=11.25° is shown in Fig. 13.

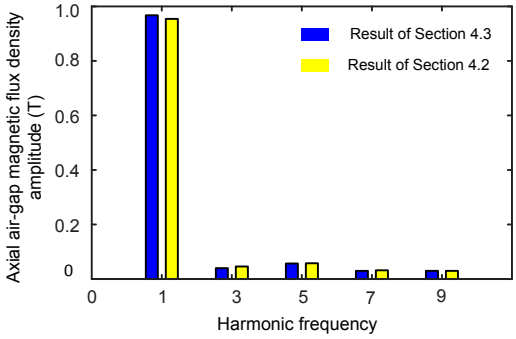

Fig. 13 Comparison of the amplitudes of the fundamental wave with each sub-harmonic

Fig. 13 shows that the novel Halbach permanent magnet array has a larger fundamental harmonic

amplitude and a smaller harmonic content compared with the optimal result of the Halbach permanent magnet array with the polar angles including the inner and outer diameters in Section 4.2. The magnetic density distribution of the novel Halbach array is shown in Fig. 14.

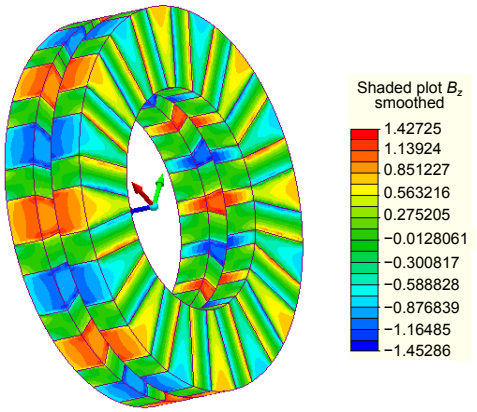

Fig. 14 Magnetic flux density distribution of the novel Halbach permanent magnet array

In summary, for a PCB stator AFPM motor with a novel Halbach permanent magnet array to ensure a permanent magnet quantity, the fundamental amplitude of air-gap flux density increased by 17.9% compared with the traditional coreless axial motors. Compared with the optimal results obtained for the Halbach permanent magnet array with polar angles including the inner and outer diameters described in Section 4.2, the fundamental amplitude of the air-gap flux density approximately increased by 3%; however, the amount of the odd harmonics, especially the three harmonics, was reduced.

5 Experiments

To verify the feasibility and accuracy of the design method and apply the novel Halbach array to verify the no-load back EMF of the motor, a prototype is required to carry out an experiment. The prototype and DC prime mover with a PCB stator are shown in Fig. 15. The test platform is shown in Fig. 16.

In this experiment, we used a power-driven 200 W DC motor as the prime mover. The amplitudes of the no-load EMF at different speeds were compared with the simulation results (Fig. 17).

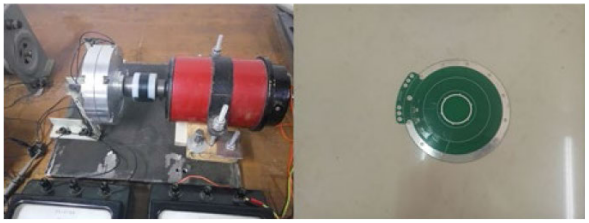

Fig. 15 PCB stator prototype and prime mover with a PCB stator

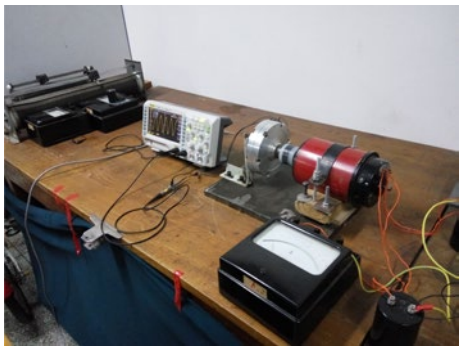

Fig. 16 Experimental platform

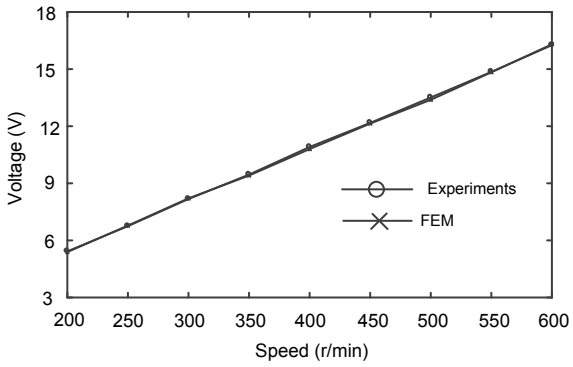

Fig. 17 Comparison between the measured values of no-load EMF amplitude and the simulation results at different speeds

The PCB stator AFPM motor was driven at a speed of 500 r/min by a coupling. No-load back EMF waveform of the PCB stator AFPM motor was measured by an oscilloscope. Experimental results are shown in Fig. 18a. The dynamic simulation results obtained using a 3D FEM are shown in Fig. 18b. Fig. 18 shows that the experimental and simulation waveforms basically follow a sinusoidal distribution, and the two waveforms are in good agreement; therefore, the finite element analysis calculation model and analysis method established in this study are reasonable.

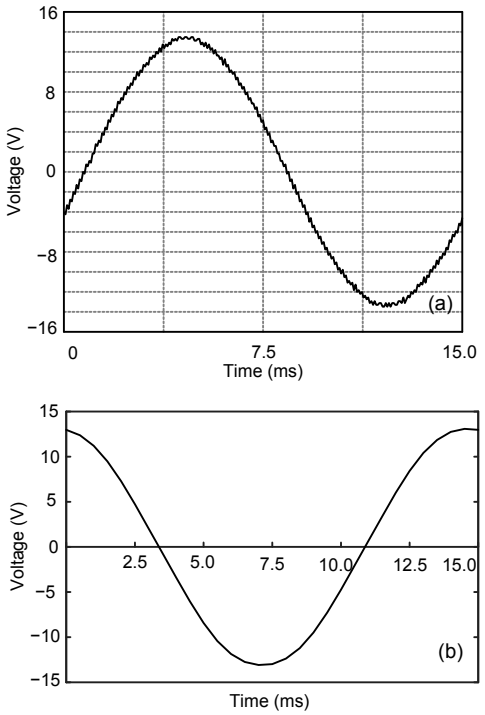

Fig. 18 Comparison of the experimental and simulation results at a speed of 500 r/min: (a) experimental results; (b) simulation results

6 Conclusions

In this paper, a novel topology for a Halbach permanent magnet array has been designed and applied to the design of a PCB stator coreless axial flux permanent magnet synchronous motor. The fundamental wave for the energy ratio as an evaluation function of the magnet design was reasonable. In the distribution of the Halbach array after changing the pole angle and adjusting the main and auxiliary poles on the magnetic steel, the magnetic pole's inner and outer diameters can be set as independent variables. The advantages of this novel array can be verified using an FEM of simulation and by prototype experiments. On the premise that the permanent magnet is unchanged, the amplitude of the air-gap flux density is increased, and the harmonic content is reduced.

For the permanent magnet pole array in the novel Halbach PCB stator AFPM motor, the main and auxiliary poles of the polar angle phase can present a larger air-gap magnetic density under the same condition; compared with the conventional AFPM permanent magnet motors, in the PCB stator motor, the magnetic flux density increased by 14.5%.

In the novel Halbach array, when assuming the magnetic pole's inner and outer diameters and the polar angle as independent variables, it is appropriate to increase the polar angle at the outer diameter and reduce the polar angle at the inner diameter of the main pole, which can further increase the air-gap flux density and reduce the magnetic leakage. For the PCB stator AFPM motor designed in this study, this amplitude was approximately 2°, and the fundamental amplitude of air-gap flux density increased by 3%.

The simulation results for the motor were in good agreement with the experimental results, showing that the finite element analysis model and the analysis method established in this study are reasonable.

References

Cao YJ, Huang RK, Jin L, et al., 2014. Design and analysis of a stator coreless axial-flux permanent magnet machine with module poles. *Proc CSEE*, 34(6):903-909 (in Chinese). https://doi.org/10.13334/j.0258-8013.pcsee.2014.06.011

Dutta R, Rahman MF, 2008. Design and analysis of an interior permanent magnet (IPM) machine with very wide constant power operation range. *IEEE Trans Energ Conv*, 23(1):25-33. https://doi.org/10.1109/TEC.2007.905061

Fan JJ, Wu JH, 2010. Analytical solution and analysis of airgap magnetic field of PMSM with partition-between-poles Halbach magnet considering effect of slotting. *Proc CSEE*, 30(12):98-105 (in Chinese). https://doi.org/10.13334/j.0258-8013.pcsee.2010.12.001

Fan JJ, Wu JH, Shen L, et al., 2009. Multi-objective optimization of permanent magnet synchronous motor with partition between poles Halbach magnet. *Trans China Electr Soc*, 24(9):53-58 (in Chinese). https://doi.org/10.3321/j.issn:1000-6753.2009.09.008

Galea M, Papini L, Zhang H, et al., 2015. Demagnetization analysis for Halbach array configurations in electrical machines. *IEEE Trans Magn*, 51(9):8107309. https://doi.org/10.1109/TMAG.2015.2429645

Huang YK, Guo BC, Guo YG, et al., 2017. Analytical modeling of axial flux PM machines with eccentricities. *Int J Appl Electromagn Mech*, 53(4):757-777. https://doi.org/10.3233/JAE-160106

Jiao ZX, Wang TY, Yan L, 2017. Design of a tubular linear oscillating motor with a novel compound Halbach magnet array. *IEEE/ASME Trans Mech*, 22(1):498-508. https://doi.org/10.1109/TMECH.2016.2611604

Kumar GLSNVAV, Jain AK, 2014. Robust design and analysis with wide speed operation of surface mounted PMSM drive. Proc IEEE Int Conf on Power Electronics, Drives and Energy Systems, p.1-6.

https://doi.org/10.1109/PEDES.2014.7042089

Kumar S, Zhao WL, Du ZS, et al., 2015. Design of ultrahigh speed axial-flux permanent magnet machine with sinusoidal back EMF for energy storage application. *IEEE Trans Magn*, 51(11):8113904. https://doi.org/10.1109/TMAG.2015.2451162

Li LL, Zhang JP, Zhang CM, et al., 2015. Research on the high efficiency external rotor permanent magnet motor based on Halbach array. Proc 18th Int Conf on Electrical Machines and Systems, p.1463-1467. https://doi.org/10.1109/ICEMS.2015.7385270

Luise F, Tessarolo A, Agnolet F, et al., 2016. Design optimization and testing of high-performance motors: evaluating a compromise between quality design development and production costs of a Halbach-array PM slotless motor. *IEEE Ind Appl Mag*, 22(6):19-32. https://doi.org/10.1109/MIAS.2015.2459118

Neethu S, Shinoy KS, Shajilal AS, 2010. Novel design, optimization and realization of axial flux motor for implantable blood pump. Joint Int Conf on Power Electronics, Drives and Energy Systems & Power India, p.1-6. https://doi.org/10.1109/PEDES.2010.5712458

Tang RY, 1997. Modern Permanent Magnet Machines. Machinery Industry Press, Beijing, China, p.310-311 (in Chinese).

Ubani OG, Mueller MA, Chick J, et al., 2016. Analysis of an air-cored axial flux permanent magnet machine with Halbach array. Proc 8th IET Int Conf on Power Electronics, Machines and Drives, p.1-6. https://doi.org/10.1049/cp.2016.0249

Wang XY, Tang RY, Du JJ, et al., 2007. Optimization of disk coreless permanent magnet synchronous motor based on Halbach—the wedgy airgap motor. *Trans China Electr Soc*, 22(3):2-5 (in Chinese). https://doi.org/10.3321/j.issn:1000-6753.2007.03.001

Wu JF, 2012. Design of a miniature axial flux flywheel motor with PCB winding for nanosatellites. Proc Int Conf on Optoelectronics and Microelectronics, p.544-548. https://doi.org/10.1109/ICoOM.2012.6316334

Yu YL, Wang YX, Sun F, 2011. Design of permanent magnet motor/generator using Halbach magnetized structure for the flywheel energy storage system. Proc 6th Int Forum on Strategic Technology, p.593-597. https://doi.org/10.1109/IFOST.2011.6021093

Zhang L, Kou BQ, Zhao BC, et al., 2013. A novel synchronous permanent magnet linear motor with Halbach secondary structure. *Trans China Electr Soc*, 28(7):39-45 (in Chinese). https://doi.org/10.3969/j.issn.1000-6753.2013.07.006

Zheng P, Zhao J, Liu RR, et al., 2010. Magnetic characteristics investigation of an axial-axial flux compound-structure PMSM used for HEVs. *IEEE Trans Magn*, 46(6):2191-2194. https://doi.org/10.1109/TMAG.2010.2042042

Zhu HQ, Chen LG, Li YW, et al, 2013. Finite element analysis of bearingless permanent magnet motors with Halbach array. *Electr Mach Contr*, 17(4):45-49 (in Chinese). https://doi.org/10.15938/j.emc.2013.04.013